Applied Surface Science 256 (2010) 4357–4364

Contents lists available at ScienceDirect

Applied Surface Science

journal homepage: www.elsevier.com/locate/apsusc

Synthesis of micro- or nano-crystalline diamond films on WC-Co substrates with various pretreatments by hot filament chemical vapor deposition

Qiu-ping Wei[a,b,c], Z.M. Yu[a,*], Michael N.R. Ashfold[b], J. Ye[a], L. Ma[c]

[a] School of Materials Science and Engineering, Central South University, Changsha, 410083, PR China
[b] School of Chemistry, University of Bristol, Bristol BS8 1TS, United Kingdom
[c] State Key Laboratory of Powder Metallurgy, Central South University, Changsha, 410083, PR China

ARTICLE INFO

Article history:
Received 20 November 2009
Received in revised form 10 January 2010
Accepted 9 February 2010
Available online 16 February 2010

Keywords:
HFCVD
Nano-crystalline diamond film
Cemented carbide
Substrate pretreatment

ABSTRACT

Diamond films deposited on tungsten carbide can lead to major improvements in the life and performance of cutting tools. However, deposition of diamond onto cemented tungsten carbide (WC-Co) is problematic due to the cobalt binder in the WC. This binder provides additional toughness to the tool but results in poor adhesion and low nucleation density of any diamond film. A two-step chemical etching pretreatment (Murakami reagent and Caro acid, (MC)-pretreatment) and a boronization pretreatment have both been used extensively to improve adhesion of CVD diamond film on WC-Co substrates. Here we discuss the applicability of MC-pretreatment for a range of Co-containing WC-Co substrates, and demonstrate a controlled synthesis process based on liquid boronizing pretreatment for obtaining smooth and dense micro- or nano-crystalline diamond films on high Co-containing WC-Co substrates. Substrate treatments and deposition parameters were found to have major influences on the smoothness, structure and quality of the diamond films. The best quality diamond films were achieved under conditions of relatively high substrate temperature (T_s) and the best adhesion was achieved at $T_s = 800\,^{\circ}C$.

© 2010 Elsevier B.V. All rights reserved.

1. Introduction

The materials used for cutting tools, sliding bearings, drawing dies and many kinds of wear resistant components are mostly cemented carbides [1]. Coatings of superhard materials are often applied to increase the useful lifespan of such tools [2–4]. Diamond possesses many unique properties, such as high hardness and wear resistance, low friction coefficient, and high chemical stability, which make diamond films grown by chemical vapor deposition (CVD) methods potentially ideal coatings for wear resistant components and high-speed dry machining applications [5–7].

CVD diamond coatings on cemented carbide tools can be used in a potentially huge market for machining non-ferrous metals and alloys, wood, chip-board, as well as hard, brittle, nonmetallic materials (e.g., ceramics, graphite, reinforced plastics) [8–10]. Since the diamond films can be directly deposited onto the substrate material, they have the advantage of being applied to tools with complex shapes. In contrast to other types of diamond tools, thin film diamond-coated tools have great potential in commercial applications due to their high performance/cost ratio [6,7].

However, the direct deposition of diamond on Co-containing cemented carbide is difficult due to the presence of cobalt at the substrate surface, which has a detrimental effect on the nucleation of diamond because it can catalyze the formation of graphite and other non-diamond carbon phases, resulting in poor film adhesion [11,12]. Many pretreatment methods, such as Co binder removal (selective Co etching), high energy ion irradiation, formation of stable Co compounds and interposition of suitable diffusion barrier layers etc., have been applied to enhance diamond nucleation by removing the surface cobalt and/or restricting the migration of cobalt to the substrate surface [13–21].

Surface roughness is one of the key factors determining the performance of diamond-coated tools. A surface with high roughness will reduce the machining precision and fields of application. Usually, the larger the grain size of the diamond film, the higher the surface roughness for the film. Nano-crystalline diamond (NCD) film has a surface with relatively low roughness, which does not require further polishing and thus can be time- and cost-effective. In addition, pollution caused by any liquid lubricants used during wet machining will be reduced by using a cutting tool with such a smooth surface [22–26].

The objective of this work is to investigate the preparation of adherent smooth diamond films on high Co-containing cemented carbide. The influence of different types of pretreatments on WC-

* Corresponding author. Tel.: +86 731 8830335; fax: +86 731 8876692.
E-mail address: zhiming@mail.csu.edu.cn (Z.M. Yu).

0169-4332/$ – see front matter © 2010 Elsevier B.V. All rights reserved.
doi:10.1016/j.apsusc.2010.02.031

13 wt.% Co substrates has been investigated, by characterizing the surface morphology and the quality of deposited diamond films using the following techniques: scanning electron microscopy (SEM), atomic force microscopy (AFM), X-ray diffraction (XRD) and Raman spectroscopy.

2. Experimental details

WC-3 wt.% Co, WC-6 wt.% Co, WC-10 wt.% Co and WC-13 wt.% Co plates (Zhuzhou Cemented Carbide Group Corporation, Hunan, China) with dimension of 12 mm × 12 mm × 5 mm were used as the substrates. The substrates were subjected to MC (Murakami reagent and Caro acid) [27] or boronization [28] pretreatments in order to study the influences of different pretreatments on the nucleation, growth and adhesion of CVD diamond film.

For the MC-pretreatment, the substrates were etched by Murakami's reagent (10 g $K_3[Fe(CN)_6]$ + 10 g KOH + 100 ml H_2O) for 15–30 min in an ultrasonic vessel in order to obtain a rough surface. The surface Co was then removed by etching in an acidic solution of hydrogen peroxide (3 ml 96 wt.% H_2SO_4 + 7 ml 40% w/v H_2O_2) for 30–60 s.

Boronization pretreatment was used with the WC-13 wt.% Co substrates only. Initially, a ceramic crucible with borax powder was put in a resistance-heated furnace and heated to the melting point of borax (740 °C). The heating temperature was then maintained for 1.5 h in the range of 750–800 °C until the borax was melted completely. The mixture powder, consisting of SiC, KCl, Na_2AlF_6, B_4C, Cr_2O_3 and active carbon, was then progressively added into the melt. The resulting mixture was then heated for 1.5 h at 950 °C. Finally, the WC-13 wt.% Co substrates were put into the crucible to react with the melt. The boronizing process was conducted at temperatures in the range of 950–1000 °C for a further 4 h.

Prior to deposition, all pretreated samples were first abraded ultrasonically in a suspension of diamond powder (<500 nm) in acetone for 15 min. This treatment is usually referred to as 'seeding', which enhances diamond nucleation either by implanting ultrafine diamond fragments into the substrate surface (on which diamond could subsequently grow during the CVD process); or by creating suitable defects on the substrate surface, which favor the inhomogeneous nucleation of diamond from the gas phase. The samples were subsequently cleaned ultrasonically with acetone and ethanol for 3 min after seeding.

A hot filament reactor system consisting of four parallel helical tungsten filaments (diameter 0.6 mm) suspended between molybdenum rods that are themselves mounted on water cooled copper frames was used for the deposition of the diamond films. The temperature of the filament (T_f) was measured by an optical pyrometer and the temperature of the substrate surface (T_s) was controlled by T_f and the filament to substrate distance. T_s was measured with two thermocouples attached to opposite edges of the substrate. Deposition parameters were set as follows: pressure: P: 10–50 Torr, T_f: 1900–2300 °C, T_s: 600–900 °C, deposition time: t: 150–300 min, ratio of methane and hydrogen (both 99.999% purity): 1–4%. In order to enhance the nucleation rate when investigating diamond film growth on boronized WC-13 wt.% Co substrates, the methane concentration was initially set to a higher value (4%, 10 min), and then reduced to 3% for subsequent growth at P = 30 Torr. No bias enhanced nucleation (BEN) was employed during the nucleation period and no argon was added into the reacting gas during the whole deposition process.

Samples were characterized with field-emission scanning electron microscopy (FE-SEM FEI, Sirion200, equipped with energy dispersed X-ray (EDX) analysis capability), atomic force microscopy (AFM NT-MDT, Solver P47), X-ray diffraction (XRD, Dmax-2500VBX with a Cu Kα radiation source (λ = 0.154 nm)) and Raman spectroscopy (LabRAM HR800). Raman spectra were recorded using the blue (λ = 488 nm) line of an Ar^+ ion laser operating at 100 mW output power. The mechanical properties of the diamond-coated WC-Co substrates were characterized using a Rockwell hardness tester with a Brale diamond indenter (angle = 120°, radius = 0.2 mm) at 600 N load. The cross-sections of the samples after indentation testing were obtained by polishing them with diamond abrasive paste and subsequently ultrasonically etching in Murakami solution for 5 min.

3. Results and discussion

3.1. Effects of MC-treatment on WC-Co substrates

In order to improve the adhesion, numerous methods have been investigated earlier [22–26], but one of the most widely used methods involves the selective etching of Co from the top surface of the WC-Co substrate prior to diamond deposition. Two-step MC-pretreatments have been proved to be conventional methods in many investigations. However, the MC-pretreatment cannot solve all problems about diamond films deposited on WC-Co substrate; it has some limitations. That is why many other pretreatment methods were been investigated since the invention of the MC-pretreatment in 1992, and hundreds more research papers published.

In this paper, the adhesion of diamond films grown onto WC-3 wt.% Co, WC-6 wt.% Co, WC-10 wt.% Co and WC-13 wt.% Co substrates was evaluated and compared by Rockwell indentation tests (600 N) conducted with a Brale indenter. The number of each sample type was 27, 50, 14 and 14, respectively, each of which were submitted to similar etching pretreatments and identical deposition conditions. Comparing all samples, 89% of the samples grown on WC-3 wt.% Co substrate exhibited good adhesion, with no flaking-off or few cracks (e.g., Fig. 1(a)). In contrast, the percentages of samples showing good adhesion on WC-6 wt.% Co, WC-10 wt.% Co, and WC-13 wt.% Co substrates were only 24%, 7% and 0%, respectively. For these four types of substrate, the rates-of-failure with severe flaking-off or large numbers of cracks (e.g., Fig. 1(b) and (c)) were, respectively, 0%, 64%, 72% and 79%. The results showed that diamond films on WC-3 wt.% Co substrates exhibited much better adhesion levels than those grown on WC-6 wt.% Co, WC-10 wt.% Co, and WC-13 wt.% Co substrates.

MC-treatment worked well for low-Co-containing cemented carbides (e.g., WC-3 wt.% Co), but once a substrate with higher Co was used, it was necessary to increase the etching time and the concentration of etching solution, and use more intense ultrasonic concussion, in order to reduce the detrimental effect of the Co in the substrate. The above treatment led to a Co-deficient, deep, loose, porous, corrosion layer on the substrate surface (Fig. 2). The removal of the Co binder phase has the effect of not only greatly decreasing the mechanical properties of the substrate surface, but also causing the formation of many deep surface pits [29–31]. This is mainly due to the fact that cemented carbides are mostly fabricated by powder metallurgy methods, where Co can easily diffuse towards the surface of the substrate during the sintering process resulting in the formation of Co agglomerates. Most of these agglomerates will transform into deep pits on the substrate surface after the two-step etching of Co. Anisotropic etching of substrates is another important cause of the deep pits.

Evidence for inhomogeneous nucleation of diamond is obvious for the samples with the WC-13 wt.% Co substrate pretreated with MC method (Fig. 3). The defects created by the MC-pretreatment enhance the diamond nucleation density, but in an inhomogeneous manner. The deep pits are not completely filled during diamond deposition and most of them remain visible on the surface of the

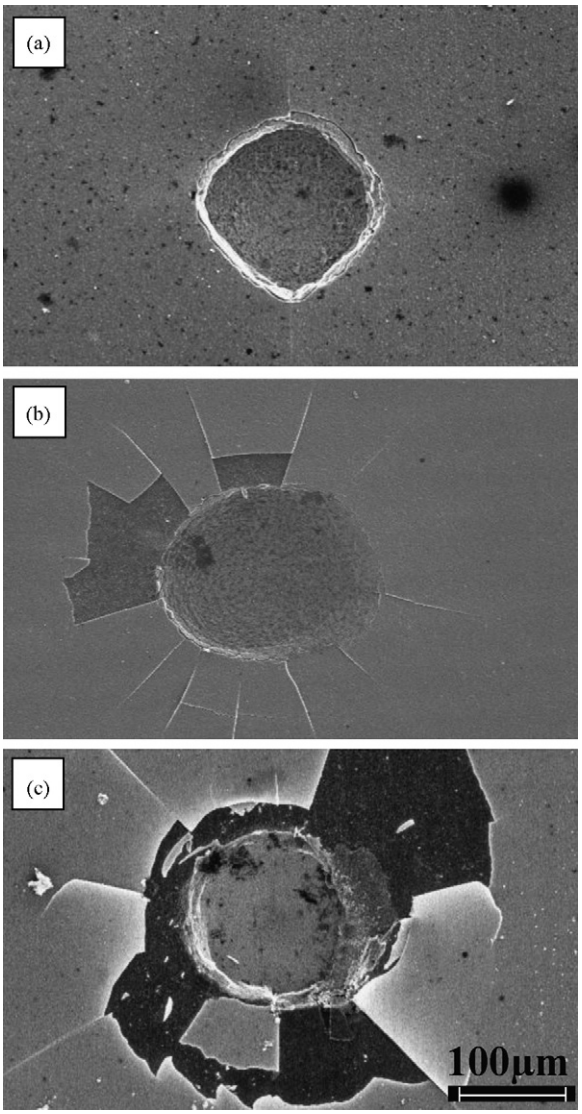

Fig. 1. SEM images of the indentation crack morphology for diamond coatings on cemented tungsten carbide substrates, illustrating (a) good adhesion and (b) and (c) severe cracking and film flaking-off.

diamond film (Fig. 4). This type of morphology will lead to an increase of the surface roughness, and a reduction of the mechanical properties and the range of applications of cutting tools coated with such film. The deep pits will likely act as sources of cracks during machining, resulting in complete failure of the tools. Further increase in growth time will allow these pits to become covered by diamond particles, but the defects will still exist at the interface. At high T_s, however, the longer growth time will give the cobalt sufficient time to diffuse to the substrate surface, as a result of the high differential concentration between the surface and the bulk. Donnet et al. [11] have demonstrated such diffusion during diamond deposition at high (>550 °C) temperatures, and the agglomeration of cobalt into ball shape structures – confirming T_s as an important parameter determining cobalt diffusion to the diamond-coated surface.

3.2. Effects of boronization treatment on WC-13 wt.% Co substrate

Boronization treatment is generally considered to be a superior method to achieve the required mechanical properties and smoothness of the substrate surface [16,17]. As described previously, the

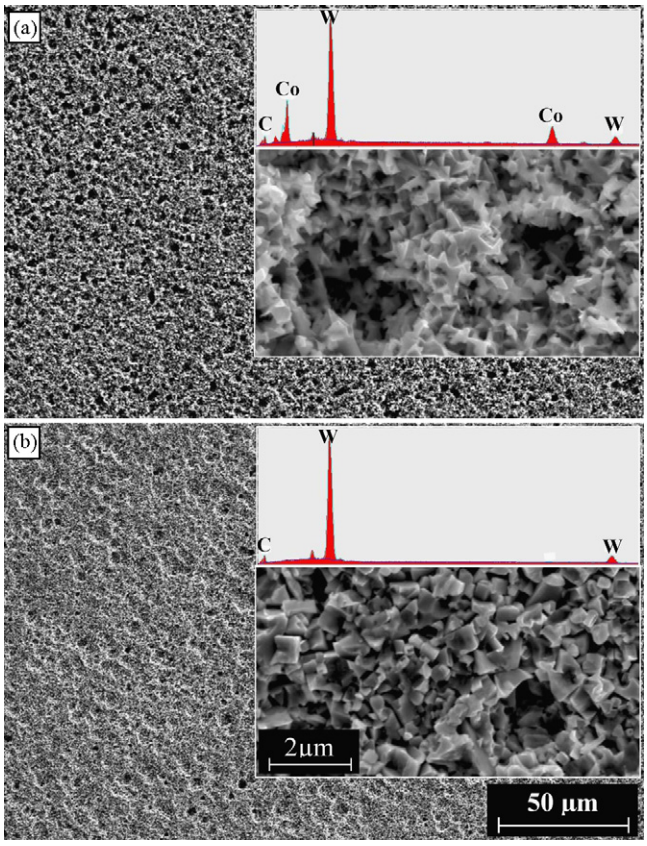

Fig. 2. SEM micrographs and EDX spectra of samples prepared by (a) $K_3[Fe(CN)_6]$: KOH: H_2O = 1:1:10 (mass proportion) ultrasonic treatment for 15 min, then (b) H_2SO_4: H_2O_2 = 3:7 (volume proportion) ultrasonic treatment for 1 min. The insets to the right show SEM images of portion of each sample recorded at higher magnification and the associated EDX spectra.

WC-13 wt.% Co substrates were sealed in a container with a molten mixture of $Na_2B_4O_7$, SiC, KCl, Na_2AlF_6, B_4C, Cr_2O_3 and active carbon and heated for 4 h. The substrates were then revealed and polished with metallographic emery paper to remove any surface residues. The samples were then etched for 60 s in a dilute acidic solution ultrasonically to allow the formation of micro-defects on the surface. AFM topographic analysis of a 3 μm × 3 μm area (not shown in this paper) reveals a random rough surface with average surface roughness (Ra) of 164 nm, root-mean-square (RMS) roughness of 220 nm.

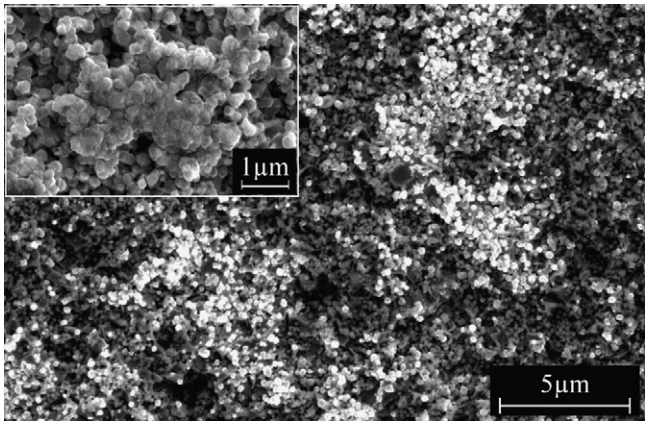

Fig. 3. SEM micrographs showing diamond nucleation on the surface of the WC-13 wt.% Co substrate with MC-pretreatment (CH_4/H_2 = 3%, P = 20 Torr, T_s = 800 °C, t = 30 min). The inset shows a portion of the sample recorded at higher magnification.

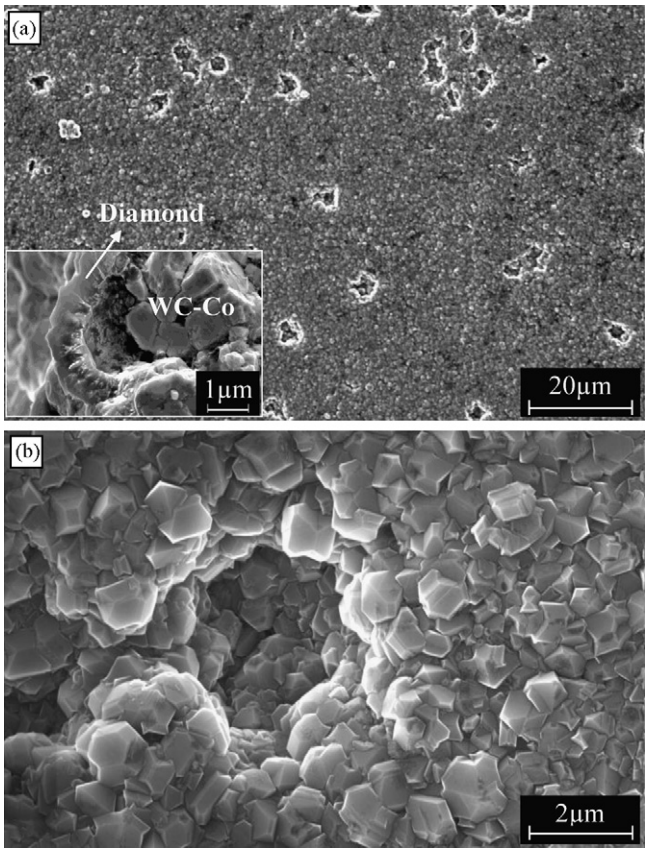

Fig. 4. SEM micrographs taken at two magnifications showing a diamond film on the surface of the WC-13 wt.% Co substrate with MC-pretreatment (CH_4/H_2 = 3%, P = 20 Torr, T = 800 °C, t = 90 min). The small image at the lower left of panel (a) is a cross-section view.

3.2.1. X-ray diffraction studies

X-ray diffraction spectra of as-received WC-13 wt.% Co and boronized WC-13 wt.% Co substrates are shown in Fig. 5(b) and (a), respectively. As Fig. 5 shows, the surface of the boronized WC-13 wt.% Co substrate mainly consists of the following phases: CoW_2B_2, WC, a small amount of CoB, and a trace amount of CoWB. No elemental Co phase could be detected from the analysis. This

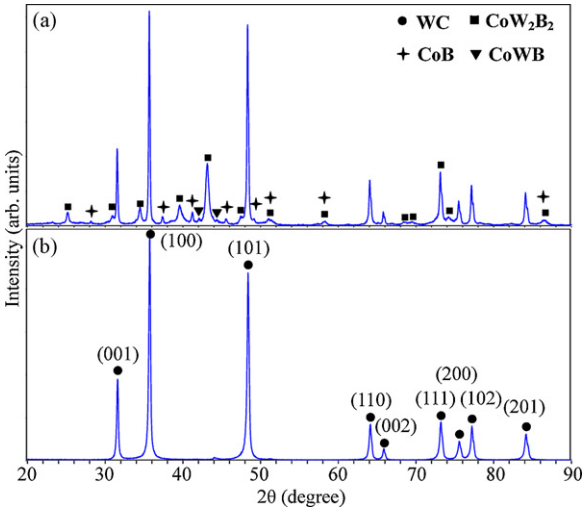

Fig. 5. X-ray diffraction peaks recorded from (a) the boronized WC-13wt% Co substrate and (b) the as-received WC-13 wt.% Co substrate. The WC peaks are labeled in (b) only.

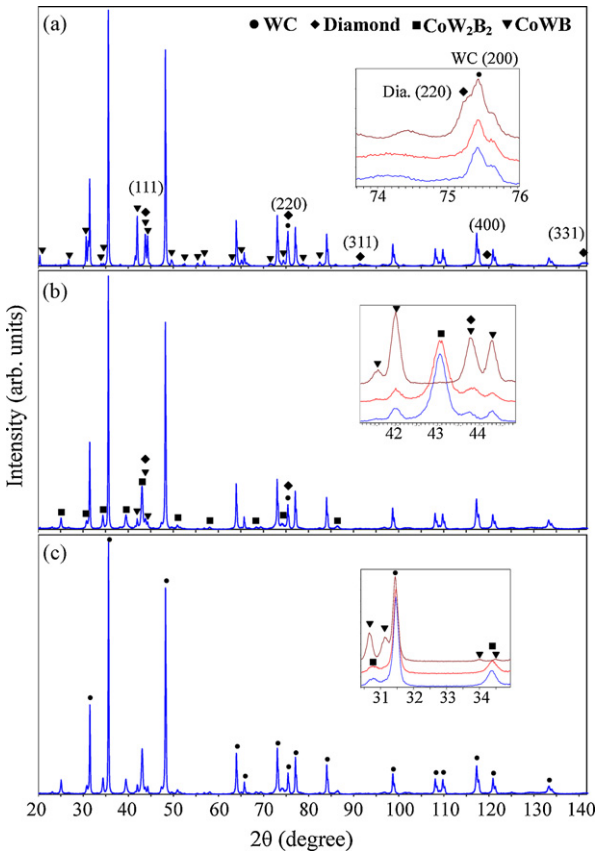

Fig. 6. X-ray diffraction patterns of diamond films deposited on boronized WC-13 wt.% Co substrates at T_s = (a) 900 °C, (b) 800 °C, (c) 700 °C (CH_4/H_2 = 3%, P = 30 Torr, t = 180 min). Peaks associated with WC are labeled in (c). The insets show detailed views of selected regions of the XRD spectra recorded at, respectively, 700 °C (bottom), 800 °C (middle) and 900 °C (top).

demonstrates that the elemental Co in the surface layer has been reacted to form inert Co-W-B phases which should not affect the diamond deposition.

X-ray diffraction patterns of diamond films deposited on the boronized WC-13 wt.% Co substrates at various T_s are shown in Fig. 6. When T_s was 700 °C (Fig. 6(c)) and 800 °C (Fig. 6(b)), no obvious phase transformation can be observed after diamond films were deposited on the substrates for 3 h. However, if T_s was 900 °C (Fig. 6(a)), obvious phase transformation occurred. In this case, most CoW_2B_2 phases have disappeared, and the major constituent becomes the CoWB phase, as is clearly evident from the inset in Fig. 6(b) and (c).

The XRD results are consistent with the view that, during the liquid boronization process, the reactive diffusion of atomic boron leads to the formation of borided structures displaying a gradient in boron content. The total amount of atomic boron decreases continuously from the surface to the interior [32]. For lower T_s (i.e., 700 °C and 800 °C) there is not enough energy to activate the cobalt atoms in the substrate in order that they diffuse to the surface. For higher T_s (i.e., 900 °C), the formation of the cobalt tungsten boride surface layer is the result of outward diffusion of cobalt atoms from the interior. Thus the composite surface layer of CoWB and CoW_2B_2 phase transforms to a layer dominated by the CoWB phase, where the reaction can be described as

$$[Co] + CoW_2B_2 \rightarrow 2CoWB \quad (1)$$

The XRD patterns in Fig. 6 further indicate the existence of the diamond. The peaks at 2θ diffraction angles of 44.0° and 75.2° are clearly revealed in the insets in Fig. 6(b) and (a). These peaks

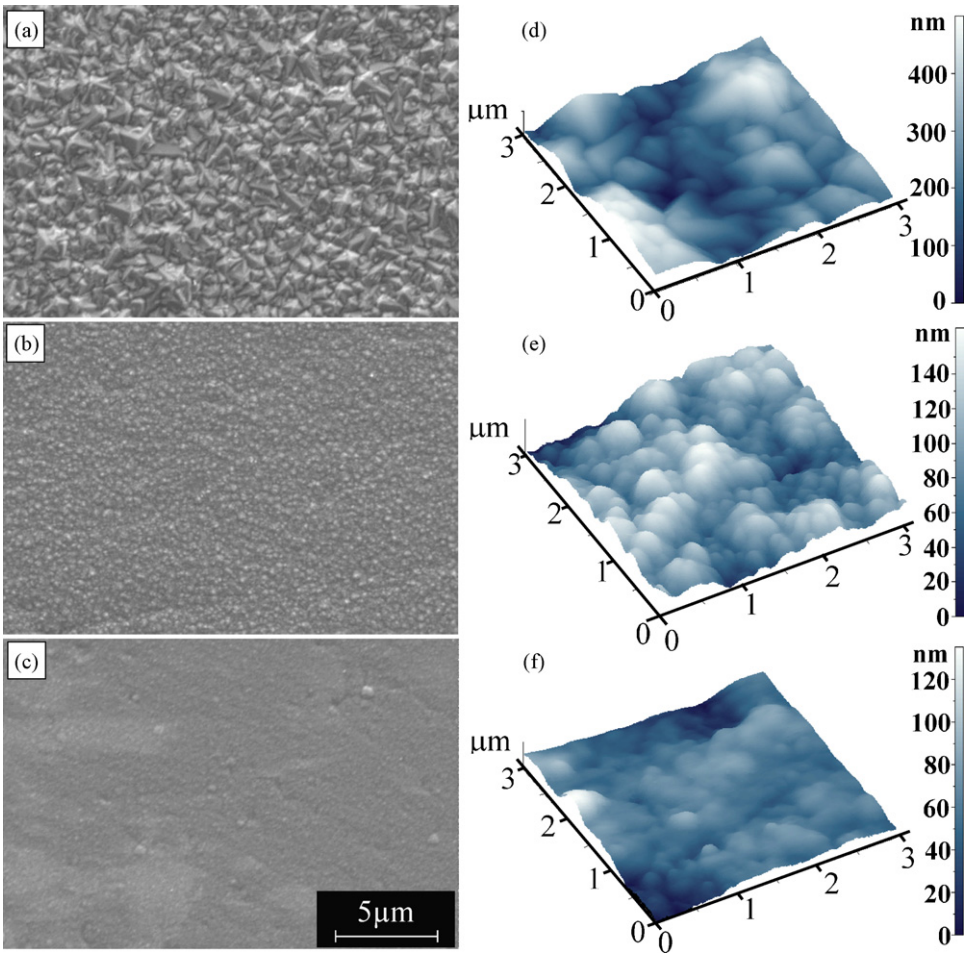

Fig. 7. Morphologies of diamond films deposited on boronized WC-13 wt.% Co substrates at T_s = (a, d) 900 °C, (b, e) 800 °C, (c, f) 700 °C. (a, b, c) and (d, e, f) are SEM and AFM images, respectively.

correspond respectively to (1 1 1) and (2 2 0) reflections associated with the cubic diamond structure. Note that the peak in the range 75.302–75.477° in the inset to Fig. 6(a) matches closely with the diamond (2 2 0) peak at 75.302° and the WC (2 0 0) peak at 75.477°. We therefore assign this peak to the overlap of the diamond (2 2 0) and WC (2 0 0) peaks. No graphite peak is discernable around 2θ = 26.48°, revealing that the film contains no significant amount of crystalline graphite. The diamond peaks become stronger and clearer with increasing T_s and are particularly clear in the T_s = 900 °C spectrum, in which the characteristic (3 1 1) and (3 3 1) reflections of diamond are also clearly evident at 2θ = 91.4° and 140.5°.

3.2.2. Investigation of surface morphology

The surface morphology of the nano-crystalline diamond films was investigated by FE-SEM and AFM (Fig. 7). When T_s = 700 °C, the surface of the diamond film exhibits a very smooth, nano-structured morphology. For T_s = 800 °C, the average grain size increases but the individual grains retain spherical morphology. With even higher T_s, the diamond film becomes rougher and the grain size also increases further. It can be clearly seen that when T_s = 900 °C, the surface of the diamond film is the roughest among the three samples. The morphologies of the diamond grains in this case are well defined and clearly observable, displaying similar features, prominent {1 1 1} places and obvious vertices. The adjacent grains are close-packed and no vacancies can be observed between them. The individual grains appear uniform and evenly distributed. The AFM topographic image of the sample grown at T_s = 900 °C (Fig. 7(a)) in a 3 μm × 3 μm area shows a random rough surface with Ra = 80 nm, RMS roughness ~99 nm, and 450 nm peak to peak separation. The corresponding values for films grown at T_s = 700 °C and 800 °C, were, respectively, Ra = 12 nm and 23 nm, RMS roughness = 17 nm and 29 nm, and peak to peak separations 135 nm and 167 nm.

The grain size distribution of the diamond films grown on boronized WC-13 wt.% Co substrates with different T_s are shown in Fig. 8. The size distribution of the particles in each case obeys Gaussian-like behavior. The size of the diamond grains increases gradually with increasing T_s. From the Gaussian fitting results, when T_s = 900 °C, the fitted Gaussian function peaks at 215 nm and has a full-width-at-half-maximum (FWHM) of ~215 nm. When T_s = 700 °C and 800 °C, the most probable diameters are respectively 58 nm and 94 nm, and the corresponding FWHM values are 27 nm and 76 nm.

3.2.3. Laser Raman analysis

X-ray diffraction is less sensitive to the presence of amorphous carbons. In contrast, Raman scattering can reveal such phases well, and is sensitive to the grain size and the crystallinity of the various carbon phases such as diamond and graphite due to the characteristic inelastic scattering processes for the different bonds and local environments. Hence, it is frequently used as an important technique to characterize CVD diamond films [25]. The Raman spectra for films deposited on boronized WC-13 wt.% Co substrates at T_s = 700 °C, 800 °C, and 900 °C are shown in Fig. 9(c), (b) and (a), respectively. These Raman spectra have been deconvoluted and analysed by multi-Gaussian peak fitting and the results are sum-

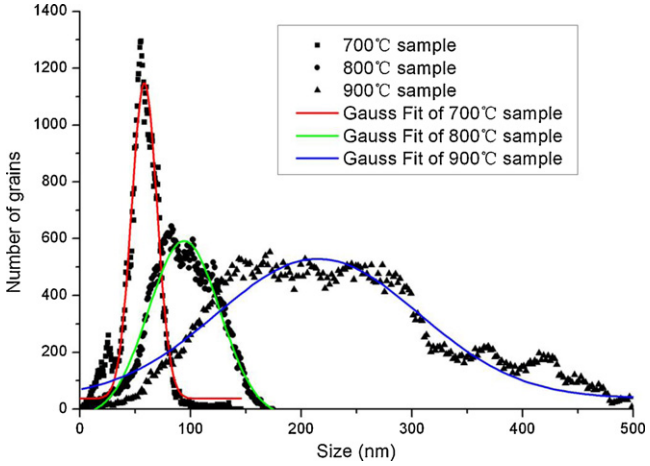

Fig. 8. The grain size distribution of the diamond films grown on boronized WC-13 wt.% Co substrates under different substrate temperatures. The grain size distribution is obtained from the AFM software, and therefore reflects the surface grain size distribution.

marized in Table 1. The proposed identification of the peaks in the table is based on Refs. [33–35].

As T_s increases from 700 °C to 900 °C, the most obvious change in the Raman spectra and the fits to these data is the disappearance of the peaks around 1150 cm^{-1} and 1490 cm^{-1}, as can be seen in Fig. 9 and Table 1. Moreover, the Raman signal at ~1332 cm^{-1}, i.e., the T_{2g} zone centre mode of the cubic diamond phase, is more pronounced in films grown at elevated temperatures. This phenomenon can be attributed directly to the transition from a nano-crystalline towards a microcrystalline diamond film structure as T_s increases from 700 °C to 900 °C. The two Raman signals at ~1150 cm^{-1} and ~1490 cm^{-1} can be attributed to trans-polyacetylene fragments mainly present at grain boundaries [34]. For decreasing T_s, the average diamond grain size decreases and the relative area of grain boundaries to diamond grain volume increases. This in turn leads to higher non-diamond carbon signals for lower substrate temperatures. In addition, Raman signals from graphitic (sp^2-bonded) carbon at both ~1350 cm^{-1} and ~1560 cm^{-1} can be observed in

Table 1
Results of multi-peak fitting the Raman spectra of diamond films deposited at T_s = 700 °C, 800 °C and 900 °C in terms of a set of Gaussian lineshape functions. Each Gaussian is defined by its centre wavenumber, full-width-half-maximum (in cm^{-1}) and height.

Peak #	Peak identification	Peak position (cm^{-1})	FWHM (cm^{-1})	Peak height (a.u.)
T_s = 700 °C (Fig. 9(c))				
1	*Trans*-polyacetylene	1142.8	36.3	1610
2	Amorphous sp^3 carbon	1205.8	185.3	1250
3	Polycrystalline diamond	1337.4	10.2	259
4	D bands of graphitic carbon	1353.2	120.3	2270
5	*Trans*-polyacetylene	1489.1	116.4	3807
6	G band for sp^2 sites	1566.7	85.8	2258
T_s = 800 °C (Fig. 9(b))				
1	*Trans*-polyacetylene	1144.4	36.9	1083
2	Amorphous sp^3 carbon	1213.1	242.9	1324
3	Polycrystalline diamond	1336.76	9.4	599
4	D bands of graphitic carbon	1354.1	120.8	2458
5	*Trans*-polyacetylene	1486.7	124.0	3794
6	G band for sp^2 sites	1567.3	93.6	3187
T_s = 900 °C (Fig. 9(a))				
1	Amorphous sp^3 carbon	1174.0	120.5	438
2	Polycrystalline diamond	1338.2	10.2	2372
3	D bands of graphitic carbon	1356.4	165.1	2107
4	G band for sp^2 sites	1552.7	133.9	2575

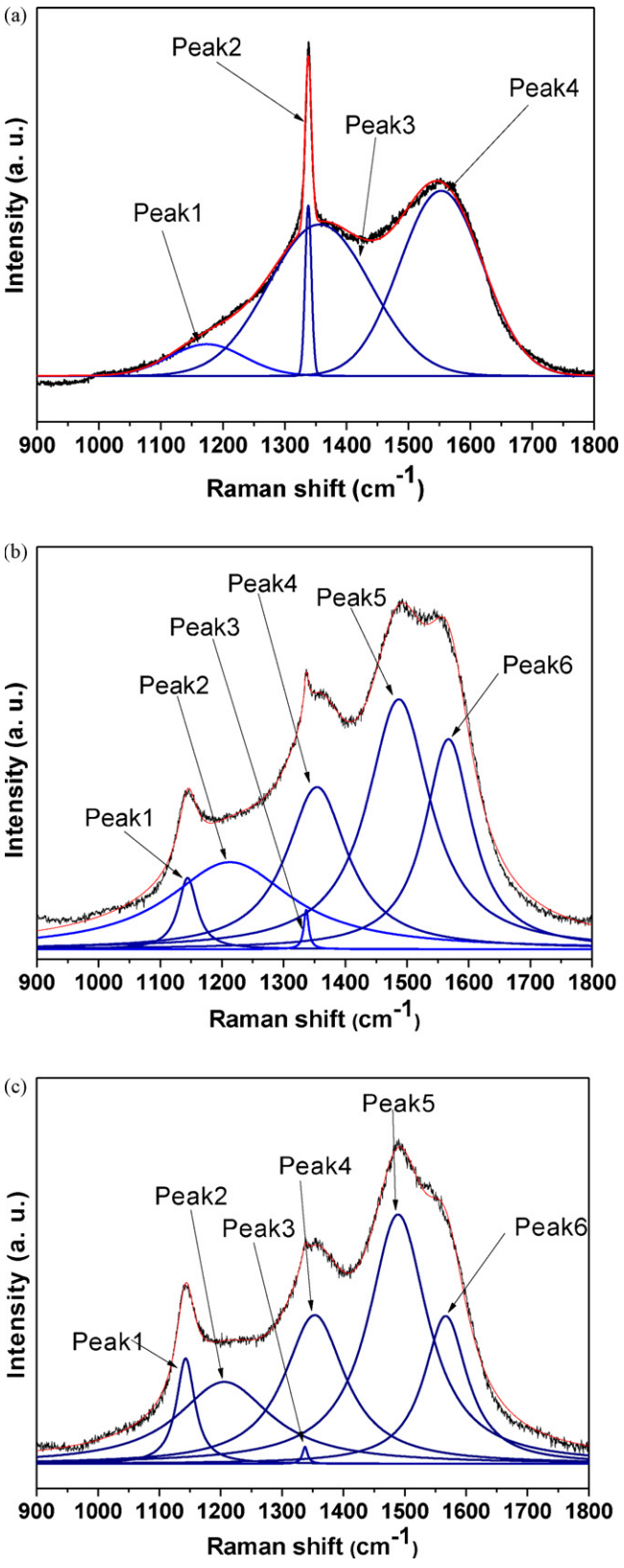

Fig. 9. Raman spectra of diamond films grown on boronized WC-13 wt.% Co cemented carbide substrates using T_s = (a) 900 °C, (b) 800 °C, (c) 700 °C (top, coarse black curve in each panel). The lower curves show the individual Gaussian lineshapes derived by spectral fitting, and their sum (top, smooth red curve in each panel).

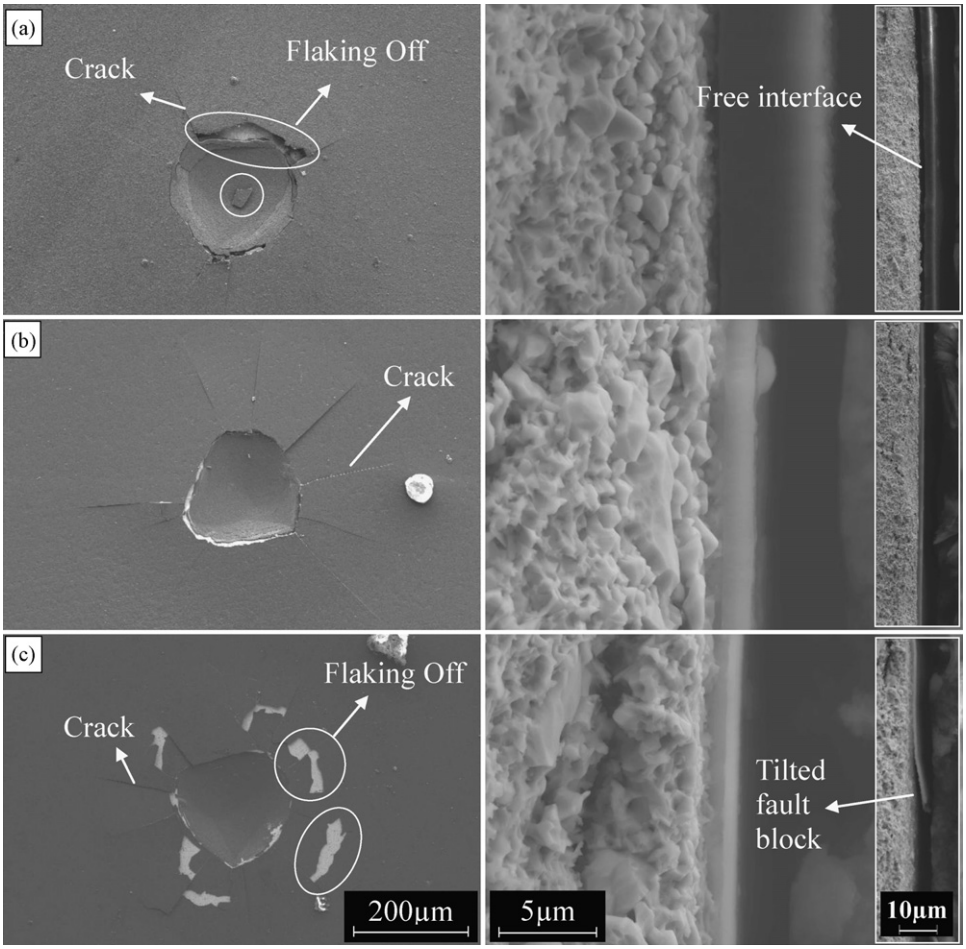

Fig. 10. SEM images of diamond films deposited at T_s = (a) 900 °C, (b) 800 °C, (c) 700 °C, after Rockwell indentation under a load of 600 N. The left hand image in each panel is a top view, while the images in the right are cross-sections, displayed at two different magnifications.

all spectra. These broad bands are the so-called D (disorder) and G (graphitic) bands, respectively [33,34], where the G mode is the stretching vibration of any pair of sp^2 sites, whether in C=C chains or in aromatic rings, and the D band arises from a breathing mode of sp^2 sites in rings not in chains.

The ratio between the diamond peak and the sp^2 characteristic bands at both ~1350 cm^{-1} and ~1560 cm^{-1} also increases with T_s, which indicates a reduction in the relative amount of sp^2-bonded carbon within the diamond films and an increase in the quality of the diamond films with increasing T_s. This observation also confirms the effectiveness of the applied boronization pretreatment in avoiding any catalytically (Co) enhanced deposition of non-diamond (sp^2-bonded) carbon phases at elevated T_s by the earlier formation of a boride surface layer.

The SEM and AFM images in Fig. 7 have already revealed the progressive increase in diamond grain size with increasing substrate temperature. Both the reduction in the D and G band signals and in the signal associated with trans-polyacetylene fragments with increasing T_s are thus a direct consequence of the increasing ratio between diamond grain volume to grain boundary surface area. This effect is likely to be enhanced by the fact that, at higher T_s, reactive etching of graphite phases by gas phase hydrogen atoms is more pronounced.

The wavenumber of the diamond peak in all of the measured Raman spectra are slightly blue-shifted with respect to the corresponding peak in natural, stress-free diamond (1332.2 cm^{-1}), which might be the result of residual, compressive stress (possibly attributable to the mismatch in thermal expansion between the substrate and diamond films), and/or due to internal film stress caused by the presence of non-diamond phases.

3.2.4. Indentation testing

In order to analyse the influence of the different crystallinity of our polycrystalline diamond films and the residual stresses acting on them, we performed Rockwell indentation tests with a total load of 600 N. Large scale flaking-off is evident with the samples grown at T_s = 700 °C as shown in Fig. 10(c) in plan view (left) and cross-section (at two different image resolutions, right). Many long cracks are also found around the indentation site. No flaking-off is observed for samples grown at T_s = 800 °C (Fig. 10(b)), but many long cracks remain observable around the indentation. In contrast, slight flaking-off can be found for the T_s = 900 °C samples, but only a few short cracks are observed. Thus it appears that best adhesion with respect to indentation tests is achieved for samples grown at T_s = 900 °C. However, the cross-section results (Fig. 10, right hand images) suggest somewhat different trends. When T_s = 700 °C, the diamond film shows extensive delamination from the substrate. This is in agreement with the indentation test. A gap is discernable between the diamond film and substrate in the sample grown at T_s = 900 °C while, for the sample grown at T_s = 800 °C, no peeling or any gap is observed. The cross-section results indicate that the adhesion of diamond film grown at T_s = 800 °C is better than that at 900 °C. Because 600 N is the cracking load of the cemented carbide, substrate generated cracks are inevitable under this load. The cracking behavior of the diamond film and the substrate is synchronous, which demonstrates the shearing force in the diamond film is not

separated from the substrate when T_s = 800 °C. However, the shearing force in the diamond film is separated from the substrate when T_s = 900 °C, where crack propagation in the film and the substrate are independent. In this case, the lengths of the cracks are shown to be reduced. We have also performed indentation tests under a load of 1500 N. Since the elemental Co in the surface layer has been pre-reacted to form inert borides, and the borides are hard materials, the boronized surface is harder than WC-Co substrate. When indenting with a 1500 N load, the cemented carbide around the indentation breaks-up. The diamond films in the centre of indentation do not peel-off, however. We cannot determine the effect of T_s on adhesion by these indentations.

For higher T_s, there is higher stress due to the thermal expansion mismatch (which has a negative influence on film adhesion) and the film is thicker. For lower T_s, there is generally poorer adhesion, due to insufficient bond formation and elemental diffusion along the film-substrate interface. This might weaken the diamond film bonding with the WC-Co substrate. There is also a higher fraction of non-diamond (sp^2-carbon) phases present within the film grown at T_s = 700 °C, and probably also at the film-substrate interface. The cracking resistance of these diamond films is likely to be a function of these non-diamond phases.

4. Conclusions

In this paper, the effectiveness of MC and boronization pretreatment for preparing Co-containing WC substrates for subsequent diamond coating by CVD methods are compared. MC-pretreatment is simple and cheaper, and shown to work well for substrates containing low (≤3%) cobalt fractions. Boronization pretreatment, in contrast, is found to be effective for much Co-richer substrates also.

Boronization pretreatment is shown to offer an increase in the nucleation density of HFCVD deposited diamond films, where the negative effects of Co are suppressed by the formation of stable cobalt boride compounds that effectively by block the outward migration of cobalt atoms at relatively high temperature. Nano-crystalline diamond films were obtained on borided high Co-containing cemented carbide substrates without use of a bias enhanced nucleation step. X-ray diffraction analysis showed that there is a strong phase transformation of the boronized samples under the applied diamond HFCVD growth conditions, especially when T_s = 900 °C, with the CoW_2B_2 phases entirely transformed to CoWB phases. Compared to the surface Co etching and the interlayer deposition techniques, boronization pretreatment offers the following advantages: (a) it guarantees the smoothness and mechanical properties of the substrate surface; (b) it avoids any matching problem between the substrates and the interlayer; (c) it prevents the diffusion of Co atoms to the surface under high substrate temperatures (T_s = 900 °C) by utilizing the phase transformation between the Co-rich and Co-poor phases.

Morphological and micro-structural analysis of the diamond films grown on the borided WC-Co samples showed that there is a gradual transition from nano-crystalline towards microcrystalline diamond films for increasing substrate temperature in the range 700–900 °C. Morphology analysis and indentation tests indicated an optimum deposition condition at T_s = 800 °C. Thus a suitable combination of substrate pretreatment and deposition condition is crucial for obtaining diamond film coatings with desirable quality and performance.

Acknowledgements

The authors wish to thank “Zhuzhou Cemented Carbide Group Corporation”, “State Key Laboratory of Powder Metallurgy”, “Innovation Foundation for Postgraduate of Hunan Province of China”, and “Open Fund for Valuable Instrument of Central South University” for the financial support.

References

[1] Y.P. Ma, F.H. Sun, H.G. Xue, Z.M. Zhang, M. Chen, Diamond Relat. Mater. 16 (2007) 481.
[2] R.F. Ávila, C. Godoy, A.M. Abrão, M.M. Lima, Wear 265 (2008) 49.
[3] G.R. Santos, D.D. Costa, F.L. Amorim, R.D. Torres, Surf. Coat. Technol. 202 (2007) 1029.
[4] R. Weissenbacher, R. Haubner, Int. J. Refract. Met. Hard Mater. 24 (2006) 374.
[5] M. Wernery, R. Locher, Rep. Prog. Phys. 61 (1998) 1665.
[6] P.W. May, Phil. Trans. R. Soc. Lond. A 358 (2000) 473.
[7] S. Ferro, J. Mater. Chem. 12 (2002) 2843.
[8] R. Polini, F. Casadei, P.D. Antonio, E. Traversa, Surf. Coat. Technol. 166 (2003) 127.
[9] G. Cabral, J. Gäbler, J. Lindner, J. Grácio, R. Polini, Diamond Relat. Mater. 17 (2008) 1008.
[10] J.P. Davim, F. Mata, Mater. Des. 29 (2008) 1568.
[11] J.B. Donnet, D. Paulmier, H. Oulanti, T. Le Huu, Carbon 42 (2004) 2215.
[12] M.A. Neto, E. Pereira, Diamond Relat. Mater. 15 (2006) 465.
[13] V. Buck, F. Deuerler, H. Kluwe, B. Schmiler, Int. J. Refract. Met. Hard Mater. 20 (2002) 101.
[14] S.K. Sarangi, A. Chattopadhyay, A.K. Chattopadhyay, Appl. Surf. Sci. 254 (2008) 3721.
[15] B. Sahoo, A.K. Chattopadhyay, Diamond Relat. Mater. 11 (2002) 1660.
[16] W. Tang, Q. Wang, S. Wang, F. Lu, Diamond Relat. Mater. 10 (2001) 1700.
[17] W. Tang, Q. Wang, S. Wang, F. Lu, Surf. Coat. Technol. 153 (2002) 298.
[18] R. Polini, M. Barletta, Diamond Relat. Mater. 17 (2008) 325.
[19] J.P. Manaud, A. Poulon, S. Gomez, Y. Le Petitcorps, Surf. Coat. Technol. 202 (2007) 222.
[20] Y.S. Li, Y. Tang, Q. Yang, S. Shimada, R. Wei, K.Y. Lee, A. Hirose, Int. J. Refract. Met. Hard Mater. 26 (2008) 465.
[21] Y.F. Huang, H.N. Xiao, Z.B. Ma, J.H. Wang, P.Z. Gao, Surf. Coat. Technol. 202 (2007) 180.
[22] F.H. Sun, Z.M. Zhang, M. Chen, H.S. Shen, Diamond Relat. Mater. 12 (2003) 711.
[23] X.M. Meng, W.Z. Tang, L.F. Hei, C.M. Li, S.J. Askari, G.C. Chen, F.X. Lu, Int. J. Refract. Met. Hard Mater. 26 (2008) 485.
[24] S.J. Askari, G.C. Chen, F.X. Lu, Mater. Res. Bull. 43 (2008) 1086.
[25] S.J. Askari, G.C. Chen, F. Akhtar, F.X. Lu, Diamond Relat. Mater. 17 (2008) 294.
[26] X.M. Meng, S.J. Askari, W.Z. Tang, L.F. Hei, F.Y. Wang, C.S. Jiang, F.X. Lu, Vacuum 82 (2008) 543.
[27] M.G. Peters, R.H. Cummings, European Patent 0519587 A1 (1992).
[28] J.A. Sue, Z. Fang, A.C. White, US Patent 6,478,887 B1 (2002).
[29] K. Vandierendonck, C. Quaeyhaegens, M. Nesladek, J.D. Haen, J. Vlekken, M. D'Olieslaeger, L.M. Stals, Surf. Coat. Technol. 74–75 (1995) 819.
[30] H. Sein, W. Ahmed, C. Rego, Diamond Relat. Mater. 11 (2002) 731.
[31] W. Ahmed, H. Sein, N. Ali, J. Gracio, R. Woodwards, Diamond Relat. Mater. 12 (2003) 1300.
[32] J.G. Buijnsters, P. Shankar, P. Gopalakrishnan, W.J.P. van Enckevort, J.J. Schermer, S.S. Ramakrishnan, J.J. ter Meulen, Thin Solid Films 426 (2003) 85.
[33] A.C. Ferrari, J. Robertson, Phys. Rev. B 64 (2001) 075414.
[34] A.C. Ferrari, J. Robertson, Phys. Rev. B 63 (2001) 121405.
[35] R. Mills, J. Sankar, A. Voigt, J. He, P. Ray, B. Dhandapani, Thin Solid Films 478 (2005) 77.